Copper complexes as biomimetic models of catechol oxidase: mechanistic studies

Koval, I.A.

6 | Proton NMR spectroscopy and magnetic properties of a solution-stable dicopper(II) complex bearing a single μ-hydroxo bridge.[†]

The reaction of copper(II) perchlorate with the macrocyclic ligand [22]py4pz (9,22-bis(2-pyridylmethyl)-1,4,9,14,17,22,27,28,29,30-decaazapentacyclo-[22.2.1.1^{4,7}.1^{11,14}.1^{17,20}]triacontane-5,7(28),11(29),12,18,20(30),24(27),25-octaene) in the presence of base leads to the formation of a dinuclear complex [Cu_2([22]py4pz)(μ-OH)](ClO_4)$_3$·H_2O, in which two copper ions are bridged by a single μ-hydroxo bridge. Each copper ion is further surrounded by four nitrogen atoms of the ligand. The μ-hydroxo bridge mediates a strong antiferromagnetic coupling ($2J$ = -691(35) cm^{-1}) between the metal centers, leading to relatively sharp and well-resolved resonances in the ^{1}H NMR spectrum of the complex in solution. In this chapter, the crystal structure, the magnetic properties and the full assignment of the hyperfine-shifted resonances in the NMR spectrum of the complex, as well as the determination of the exchange coupling constant in solution through temperature-dependent NMR studies, are reported.

[†]This chapter is based on: Koval, I. A., van der Schilden, K., Schuitema, A. M., Gamez, P., Belle, C., Pierre, J.-L., Luken, M., Krebs, B., Roubeau, O., Reedijk, J., Inorg. Chem., 2005, 44, 4372-4382

6.1 Introduction

As can be concluded from Chapter 4, one of the factors strongly influencing catecholase activity of dicopper(II) complexes is the bridging ligand between the metal centers. As discussed in Chapter 1, many authors have pointed out that *i.e.* hydroxo-bridged dicopper(II) complexes exhibit catecholase activity, partially due to the ability of the hydroxide anion to facilitate the deprotonation of catechol and thus promote its binding to the copper(II) ions.[1-4] On the other hand, the presence of strongly binding ligands, *e.g.* halogen atoms, prevents their displacement by the incoming catecholate and thus hampers the catalytic cycle.[5]

Consequently, a new dinuclear copper(II) complex $[Cu_2([22]py4pz)(\mu\text{-}OH)](ClO_4)_3 \cdot H_2O$ (**1**) with the macrocyclic ligand [22]py4pz (Figure 6.1) has been prepared and structurally characterized.[6] This ligand has been designed earlier to model the active site of the structurally related type-3 copper protein hemocyanin.[6,7] It is able to keep two copper ions in a close proximity and to provide each of them with four nitrogen donor atoms from pyridine and pyrazole rings and the tertiary amine groups. In dicopper(II) complex **1** two copper ions are kept together by the macrocyclic moiety, each copper ion being surrounded by four nitrogen donor atoms from the ligand. In addition, the copper(II) ions are bridged by a single hydroxo bridge. The structure of the complex is thus fairly similar to the *met* form of the active site of catechol oxidase.[8] Considering proton NMR as a powerful spectroscopic tool to study paramagnetic copper(II) complexes in solution, the magnetic properties, as well as ^1H NMR studies of the paramagnetic complex **1**, have been studied in depth and are reported in this chapter.

6.2 Results and discussion

6.2.1 Synthesis and physical properties of 1

The reaction scheme of the synthesis of the macrocyclic ligand [22]py4pz is depicted in Figure 6.1.[6] The dinuclear complex $[Cu_2([22]py4pz)(\mu\text{-}OH)](ClO_4)_3 \cdot H_2O$ was prepared by reaction of $Cu(ClO_4)_2 \cdot 6H_2O$ and the ligand [22]py4pz in acetonitrile in the presence of one equivalent of NMe_4OH. Small green crystals of the compound, suitable for X-ray single crystal analysis, were obtained by slow diethyl ether diffusion in an acetonitrile solution of the complex. The complex was found to be moderately soluble in acetonitrile and DMSO, poorly soluble in water, and completely insoluble in other common solvents.

The UV-Vis-NIR spectrum of the complex in CH_3CN solution exhibits two absorption bands at 350 nm (ε = 7176 $M^{-1}cm^{-1}$) and at 821 nm (ε = 336 $M^{-1}cm^{-1}$). The first one corresponds to the charge transfer band from the hydroxo bridge to the copper ions, whereas the second one is assigned to a d-d transition band of Cu^{II} ions. The complex is EPR silent both in the solid state and in acetonitrile solution at 77 K.

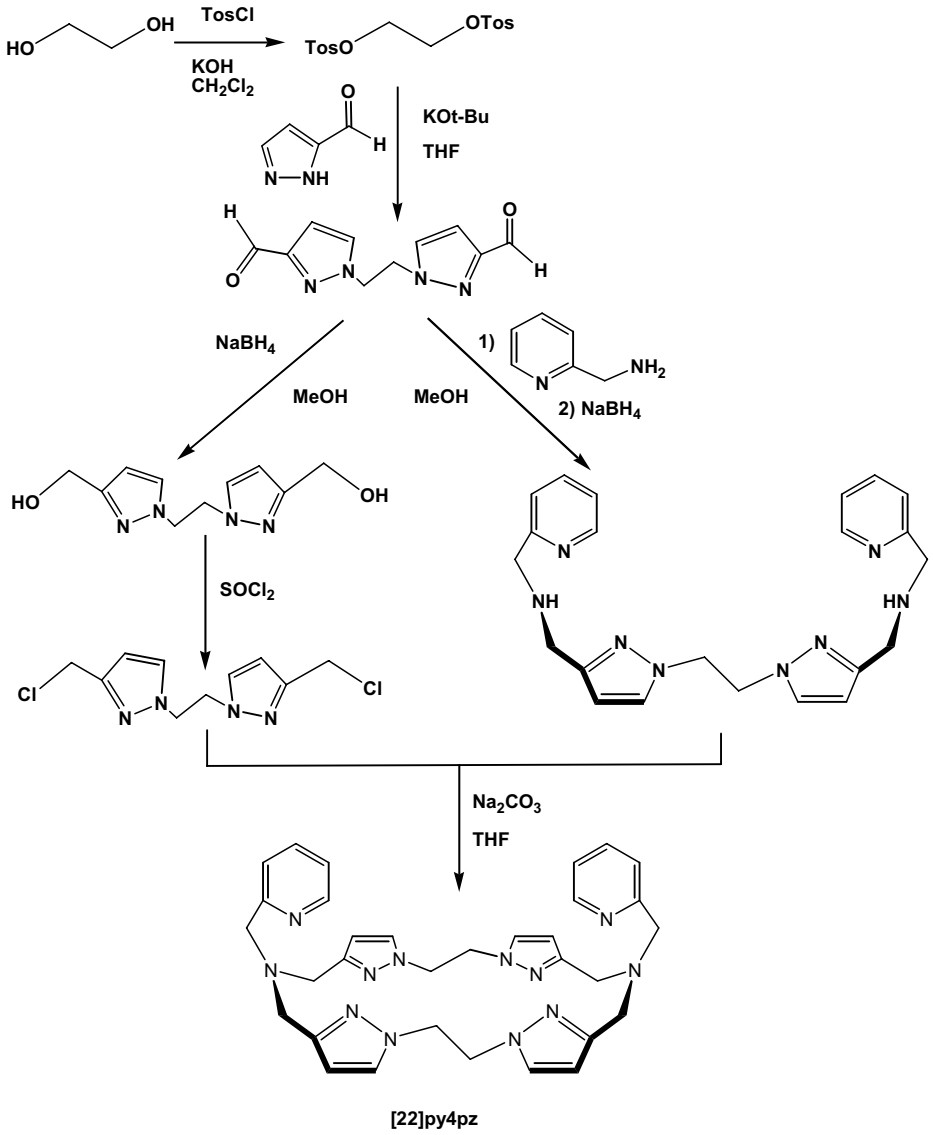

Figure 6.1. The scheme of the synthesis of the macrocyclic ligand [22]py4pz (9,22-bis(2-pyridylmethyl)-1,4,9,14,17,22,27,28,29,30-decaazapentacyclo-[22.2.1.1^{4,7}.1^{11,14}.1^{17,20}]triacontane5,7(28),11(29),12,18,20(30),24(27),25-octaene).[6,7]

6.2.2 Crystal structure description of 1

The ORTEP projection of 1 is depicted in Figure 6.2. Selected bond distances and bond angles are presented in Table 6.1. The Cu^{II} ion is in an N_4O environment, which can be best described as a distorted trigonal bipyramid with a τ value of 0.83 (τ = 1 for the trigonal bipyramidal geometry and 0 for the square pyramidal geometry).[9] The equatorial positions are occupied by the two pyrazole nitrogen atoms, N3 and N10 at distances of, respectively, 2.033(3) Å and 2.072(3) Å, and the pyridine N18 atom at a distance of 2.087(4) Å. The bridging O23 atom at a distance of 1.9215(12) Å and the tertiary amine N15 atom at a distance of 2.065(3) Å are occupying the axial positions. The small N3-Cu1-N15 and N15-Cu1-N10 angles of 80.17(13) and 80.94(13)º,

respectively, are imposed by the three-bond ligand bites. The bridging oxygen atom O23 from the hydroxide anion connects the two central copper atoms Cu1 and Cu1b, whereby the macrocycle adopts a *cis*-(boat)-conformation. The two pyridine groups are located at the same side above the macrocyclic ring and the two Cu^{II} ions lie almost in the plane of the ring with a Cu…Cu distance of 3.7587(11) Å. The Cu-O-Cu angle is 156.0(3) Å.

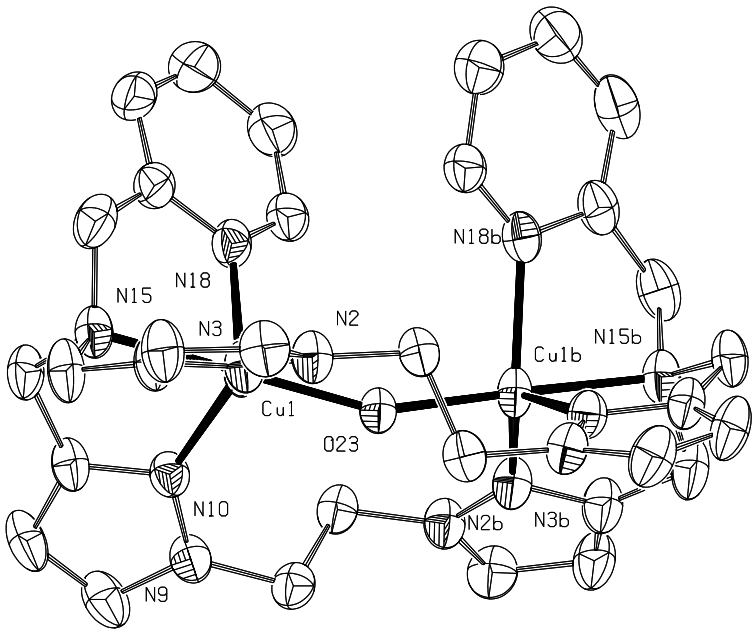

Figure 6.2. ORTEP representation of the complex cation $[Cu_2([22]py4pz)(\mu\text{-}OH)]^{3+}$ (symmetry code: b = -x, y, 1/2-z). Hydrogen atoms are omitted for clarity.

Table 6.1. Selected bond lengths and angles for $[Cu_2([22]py4pz)(\mu\text{-}OH)](ClO_4)_3 \cdot H_2O$ (**1**).

Bond lengths (Å)			
Cu1 - O23	1.9215(12)	Cu2 - N10	2.072(3)
Cu1 - N3	2.033(3)	Cu2 - N18	2.087(4)
Cu1 - N15	2.065(3)		
Bond angles (°)			
O23 - Cu1 - N3	98.55(11)	N15 - Cu1 - N10	80.94(13)
O23 - Cu1 - N15	178.60(14)	O23 - Cu1 - N18	100.85(16)
N3 - Cu1 - N15	80.17(13)	N3 - Cu1 - N18	122.50(14)
O23 - Cu1 - N10	99.49(11)	N15 - Cu1 - N18	80.36(14)
N3 - Cu1 - N10	128.73(13)	N10 - Cu1 - N18	100.38(13)

6.2.3 Magnetic behavior of 1

The temperature dependence of the molar magnetic susceptibility χ_M and its inverse $1/\chi_M$ deduced from measurements at 1000 Oe (0.1 Tesla) are given in Figure 6.3 (left). The molar magnetic susceptibility χ_M of compound **1** at 350 K equals to *ca.*

5×10^{-4} cm^3mol^{-1}, about half of the expected value for two uncoupled S =1/2 centres (*ca.* 1×10^{-3} cm^3mol^{-1}), thus indicating a strong antiferromagnetic coupling between the copper(II) ions. Upon lowering the temperature, χ_M further decreases to reach a plateau at *ca.* 1.5×10^{-4} cm^3mol^{-1} below 150 K. At temperatures below 100 K, the behaviour is dominated by a Curie tail, typical of a small paramagnetic impurity, as often found in molecular copper compounds. The presence of a small paramagnetic impurity is confirmed by measurements against the applied field at 5 and 100 K (Figure 6.3, right). To evaluate the strength of the magnetic interaction between the copper(II) ions within the dimeric unit in **1**, the following expression for the susceptibility, based on the Hamiltonian $H = -2J\,S_1S_2$ was thus used (equation 6.1):[10]

(6.1)

$$\chi = (1-p)\frac{2N_A\beta^2g^2}{k_BT\left[3+\exp\left(-\frac{2J}{k_BT}\right)\right]} + p\frac{N_A\beta^2g^2}{2k_BT} + TIP$$

where $2J$ corresponds to the singlet-triplet energy gap, p represents the amount of paramagnetic impurity and TIP a Temperature Independent Paramagnetism term. The fitting was performed fixing g to 2 and the best-fit parameters were then $2J$ = –691(35) cm^{-1}, TIP=$1.0(1)\times10^{-4}$ cm^3mol^{-1} and p=0.63(1)%. The large error bar on $2J$ originates from the lack of data at higher temperatures at which the maximum in χ_M would be observed.

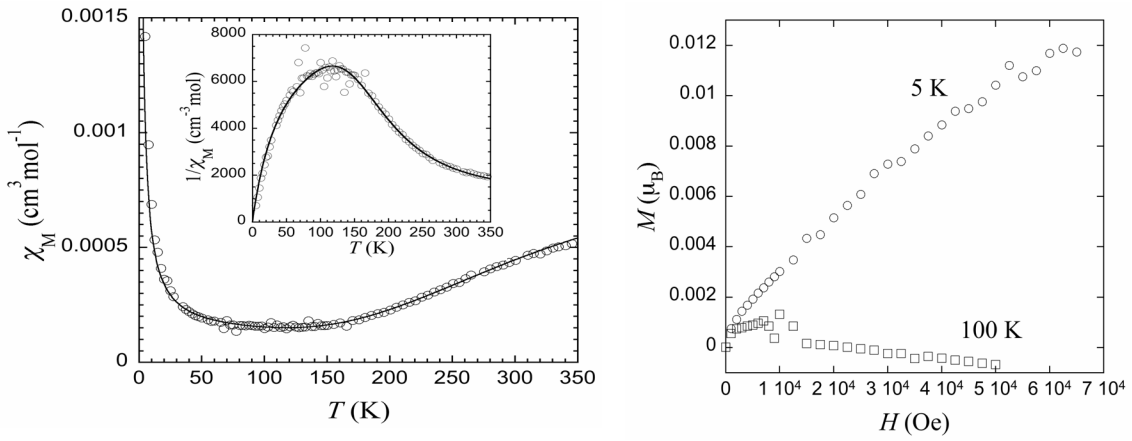

Figure 6.3. Left: magnetic susceptibility data χ and 1/χ *vs.* T for **1** in the temperature range 5-350 K in a 1000 Oe (0.1 Tesla) applied field. The full lines correspond to the best fit to a dimer model (see text). Right: field dependence of the magnetization of **1** at 5 and 100 K, showing the presence of a small paramagnetic impurity, in agreement with the variable-temperature data. The data were corrected for diamagnetism of the sample.

From the magneto-structural viewpoint, dinuclear copper complexes with a single hydroxo bridge are still rare, given the extensive research devoted to copper(II) coordination compounds. In all cases, antiferromagnetic exchange couplings have been observed, the strength of which depends on structural parameters. Attempts to derive

magneto-structural correlations were undertaken recently[11] for monohydroxo-bridged copper(II) ions in a square-planar environment. It was found that the antiferromagnetic exchange coupling increases with the Cu–O–Cu angle. Indeed for such geometry, the σ overlap of the spin-rich $d_{x^2-y^2}$ orbitals increases with Cu–O–Cu angles closer to 180º. In **1**, however, the Cu^{II} ions are in a trigonal bipyramidal environment with the hydroxo bridge in axial position. Furthermore, besides square-pyramidal and trigonal bipyramidal surroundings, monohydroxo-bridged dicopper(II) species are also found in the literature in combination with other bridging ligands, and with tetrahedral, square pyramidal, or octahedral environments, various types of distortions, and different coordination site for the hydroxo bridge. Therefore, the reported magneto-structural data for dinuclear compounds in which the Cu^{II} ions are only bridged by one hydroxo group, and for which the geometry around the Cu^{II} ions can be reasonably described by a type of coordination sphere, have been gathered in Table 6.2 and Figures 6.4 and 6.5. Cases for which the spin density at the hydroxo coordination site is expected to be negligible, *e.g.* for the hydroxo-bridging group in axial position in a square-pyramidal geometry, have been excluded.

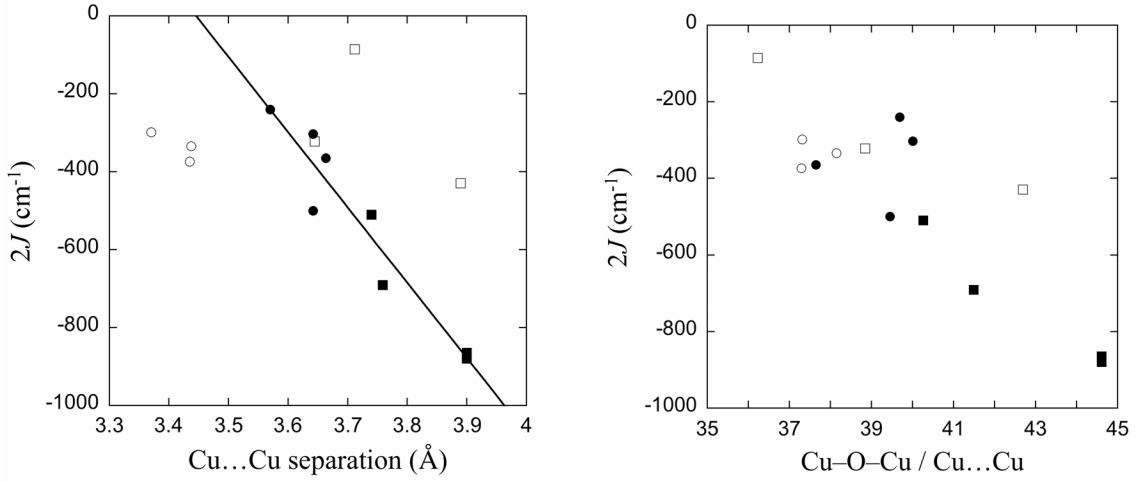

Figure 6.4. Correlation of the singlet-triplet energy gap 2*J* in monohydroxo-bridged dicopper(II) complexes with the Cu…Cu separation (left), and with the ratio Cu–O–Cu angle over Cu…Cu separation (right). Empty circles represent the square planar geometry, full circles the square pyramidal geometry with OH group in the equatorial position, full squares the trigonal bipyramid geometry with OH group in the axial position and empty squares the trigonal bipyramid geometry with OH group in the equatorial position. The full line is a linear fit (Eq. $-2J = 6653.8 - 1931.3 \times$Cu…Cu) of the data concerning compounds with the trigonal bipyramid geometry and the hydroxo bridge in the axial position and the square pyramidal geometry with the hydroxo bridge in the equatorial position.

Table 6.2. Magneto-structural data of relevant dicopper(II) complexes with a single hydroxo bridge. 2*J* represents here the singlet-triplet energy gap. SPl = square planar, Spy = square pyramidal with OH^- in the equatorial position, TBPax = trigonal bipyramid with OH^- in the axial position, TPBeq = distorted trigonal bipyramid with OH^- in the equatorial position. H_2L^1 = 2,6-bis[N-(phenyl)carbamoyl]pyridine, L^2 = tetraimine Schiff base of tris(2-aminoethyl)amine and 2,5-diformylfuran, L^3 = 1,4,7,13,16,19-hexaaza-10,22-dioxatetracosane, L^4 = octaamine from BH_4^- reduction of the Schiff base of tris(2-aminoethyl)amine and 2,5-diformylfuran, L^5 = 1,1,2,2-tetrakis(2-pyridyl)ethylene, dpm = di(2-pyridyl)methane, L^6 = Schiff base of 2,6-diacetylpyridine and 3,6-dioxaoctane-1,8-diamine, dien = diethylenetriamine, terpy = 2,2',6',2''-terpyridine, L^7 = partially hydrolyzed Schiff base of 2,6-diacetylpyridine and tris(2-aminoethyl)amine, tpmc = 1,4,8,11-tetrakis(2-pyridylmethyl)-1,4,8,11-tetraazacyclotetradecane

Geometry type	*Formula*	*Cu…Cu (Å)*	*Cu–O–Cu (°)*	*Cu–O–Cu / Cu…Cu*	*2J (cm^{-1})*	*Ref.*
TBPeq	$[Cu_2(bpy)_4(OH)](ClO_4)_3$	3.645	141.60	38.85	-322	Haddad. 1981[12]
SPl	$Na[Cu_2(L^1)_2(OH)]\cdot 2H_2O$	3.437	131.11	38.15	–334	Patra, 2000[11]
SPl	$K[Cu_2(L^1)_2(OH)]\cdot 2H_2O$	3.370	125.74	37.31	–298	Patra, 2000[11]
TBPax	$[Cu_2(L^2)(OH)](ClO_4)_3\cdot 1.5H_2O$	3.740	150.60	40.27	–510	Adams, 1996[13]
TBPax	$[Cu_2([22]py4pz)OH](ClO_4)_3\cdot H_2O$	3.757	155.97	41.49	–691	This thesis
SPy	$[Cu_2(L^3)(OH)(ClO_4)](ClO_4)_2\cdot CHCl_3$	3.642	143.7	39.46	–500	Coughlin, 1981[14]
TBPax	$[Cu_2(L^4)(OH)](CF_3SO_3)_3$	3.90	174.0	44.61	–865	Lu, 1994[15]
TBPax	$[Cu_2(L^4)(OH)](CF_3SO_3)_3\cdot H_2O$	3.90	174.0	44.61	–880	Harding, 1993[16]
SPy	$[Cu_2(L^5)(dpm)(OH)](ClO_4)_3\cdot 2H_2O$	3.663	137.9	37.65	–365	Spodine, 1991[17]
SPy	$[Cu_2(L^6)(OH)](ClO_4)_2\cdot H_2O$	3.57	141.7	39.69	–240	Drew, 1981[18]
SPl	$[Cu_2(dien)_2(ClO_4)_3(OH)]$	3.435	128.1	37.29	–374	Castro, 1990[19]
SPy	$[Cu_2(terpy)_2(H_2O)(ClO_4)_3(OH)]$	3.642	145.7	40.05	–303	Folgado, 1989[20]
TBPeq	$[Cu_2(L^7)(OH)](CF_3SO_3)(BPh_4)_2$	3.89	166.1	42.70	–430	Harding, 1995[21]
TBPeq	$[Cu_2(tpmc)(OH)](ClO_4)_3\cdot 2H_2O$	3.712	134.5	36.23	–86	Asato, 1989[22]

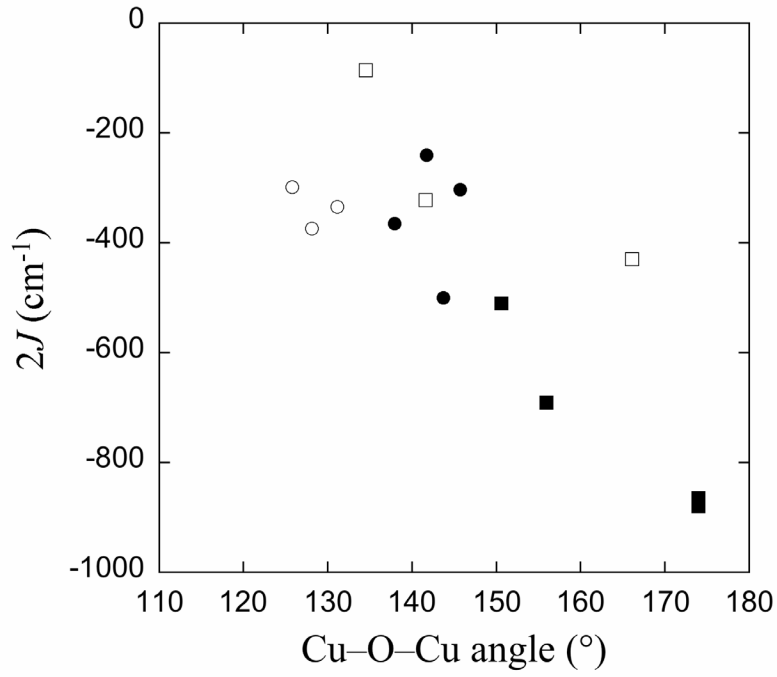

Figure 6.5. Correlation of the singlet-triplet energy gap 2*J* in mono-hydroxo-bridged dicopper(II) complexes with the Cu–O–Cu angle, (empty circles) square planar geometry, (full circles) square pyramidal geometry with OH group in equatorial position, (full squares) trigonal bipyramid geometry with OH group in axial position and (empty squares) trigonal bipyramid geometry with OH group in equatorial position.

A common general trend is observed with the singlet-triplet energy gap increasing with longer Cu…Cu separations, wider Cu–O–Cu angles and higher Cu–O–Cu/ Cu…Cu ratios. These structural parameters are obviously interdependent. For the three geometries considered, the increase in singlet-triplet energy gap in fact corresponds to a variation of the structural parameters towards situations for which the overlap between the magnetic orbitals (d_{z^2} in trigonal bipyramid, $d_{x^2-y^2}$ in square planar and square pyramid) and the hydroxo O 2p orbital is the most efficient, close to linearity. The antiferromagnetic σ-superexchange pathway through the hydroxo bridge is then the most efficient, yielding virtually diamagnetic complexes.

In addition, there is a good linear correlation between the Cu…Cu separation and the singlet-triplet energy gap among compounds having the trigonal bipyramid geometry and the hydroxo bridge in axial position and square pyramidal geometry with the hydroxo bridge in equatorial position (see Figure 6.4, left). It has to be noted that for such a monoatomic single bridge, only a small dependence on the actual Cu^{II} coordination environment can be expected, if the bridging atom lies in a spin-rich position. The correlation found here is of relevance for the characterization of mimics for dinuclear copper centres in biological systems.

6.2.4 ^{1}H NMR assignment strategy for 1

6.2.4.1 ^{1}H NMR, 2D COSY NMR and T_1 measurements

^{1}H NMR spectroscopy has only relatively recently emerged as a useful tool in studying the structural and magnetic properties of Cu^{II} coordination compounds in solution.[23-25] The slow electronic relaxation of Cu^{II} ions usually results in large line widths and poor resolution of the spectra, which makes their interpretation very difficult, if not impossible. However, if two antiferromagnetically coupled copper(II) ions are present in a complex, the situation is different. In antiferromagnetically coupled dicopper(II) systems, the ground state is a diamagnetic (S = 0) singlet. The energy separation between the ground state and the paramagnetic (S = 1) excited triplet state, which increases with the strength of the antiferromagnetic coupling, may lead to relatively sharp resonances, facilitating the spectra interpretation.[26]

In the present case, a very strong ($2J$ = -691(35) cm^{-1}) antiferromagnetic coupling between the copper(II) centers in **1** results in relatively sharp resonances with rather small hyperfine shifts, observed in a range of -50 to +30 ppm.

At room temperature, only 7 well-resolved signals are found in the region of 0-200 ppm in the ^{1}H NMR spectrum of **1** (Figure 6.6). One additional weak signal is observed at -48 ppm (Figure 6.7, left). The temperature-variable 1D spectra, recorded in the temperature interval 233-353 K (Figure 6.7, the data recorded above 293 K are not shown), reveal that the signal observed at 8.6 ppm at RT results from coincidental degeneracy of two resonances. Furthermore, two very broad signals at *ca.* 25 and 20 ppm become clearly visible at 233 K. In total, 11 resonances are thus observed in the whole spectral window (Figure 6.7), which implies the presence of an additional (pseudo-)symmetry plane in the cationic species next to the C_2 symmetry axis, observed in the crystal structure of **1**. One can imagine it connecting two tripodal nitrogen atoms, passing through both copper centers and with two pyridine rings lying virtually in the plane, resulting in the equivalency of all four pyrazole rings, all methylene groups of the ethylene moieties and the methylene N(tripodal)-C$\underline{H}_2$-pz groups. However, taking into account that the two protons (*e.g.* equatorial *vs.* axial) of the methylene groups are diastereotopic and that these usually experience different hyperfine shifts, 12 resonances are expected for **1** (it should be noted that the protons of the pyridylmethylene moieties are **not** diastereotopic, as they become symmetry-related due to the pseudo symmetry plane). In general, the protons in a close proximity to copper ions experience stronger paramagnetic effects and thus shorter longitudinal relaxation times (T_1) and broader line widths (shorter transverse relaxation times T_2) in comparison to the protons in the periphery.[24] Therefore, as shown previously for paramagnetic Cu^{II} complexes, it is not uncommon for the resonances corresponding to the protons closest to copper to broaden beyond recognition.[27,28] It can be thus tentatively proposed that the resonances corresponding to the methylene protons of the pyridylmethyl moieties, which are the

closest to copper (H16a – Cu 3.050 Å, H16b – Cu 3.728 Å), are too broad to be detected. Another explanation of the observation of only 11 signals instead of 12 would be a coincidental degeneracy of two resonances which can not be resolved at different temperatures due to the line broadness.

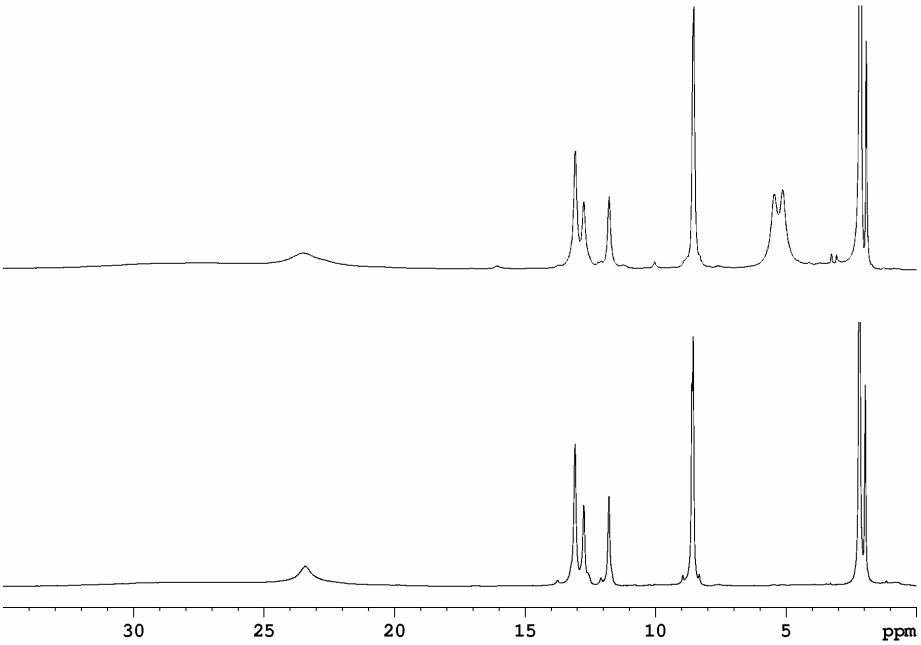

Figure 6.6. Positive range parts of the ^{1}H NMR spectra (300 MHz, CD_3CN) of **1** (top) and **1**-d_8 (the complex in which the protons of the ethylene moieties are substituted with deuterium atoms) (bottom).

The peak at -48 ppm can easily be assigned to the proton of the OH group, as it has an approximate integral intensity of 1 and disappears upon addition of D_2O to the complex solution due to a proton-deuterium exchange. Furthermore, as evidenced from the X-ray structure, the Cu d_z^2 orbital, which contains the unpaired electron, is directed along the Cu-O bond. Therefore, a spin polarization mechanism would cause the μ-hydroxo proton to be shielded and thus upfield shifted, as was previously reported for similar cases.[25] This observation is also consistent with the assignment.

The resonances E, F, G and C have been assigned to the pyridine protons according to their relative integral intensity of 2 (the intensity of C being measured at 233 K, where it appears relatively sharp). The resonances I and J, which overlap at 233 K, integrate as 4:4, as well as the resonances D and H, and the two very broad resonances A and B. However, the integration of the latter two resonances is unfortunately rather ambiguous due to the line broadness, even when measured at 233 K.

Resonances D and H have been assigned to the protons of the pyrazole rings by ^{1}H 2D COSY NMR at 263 K (Figure 6.8). The resonance G shows cross-signals with both resonances E and F, unambiguously ascribing it to the γ-protons of the pyridine rings and the resonances E and F to the *m*-pyridine protons. Resonances I and J, which do not display cross-signals in COSY, have been confirmed to originate from the

diastereotopic ethylene protons by the chemical substitution of the respective protons by deuterium. The signals in question are absent in the spectrum of the deuterated compound (Figure 6.6, bottom).

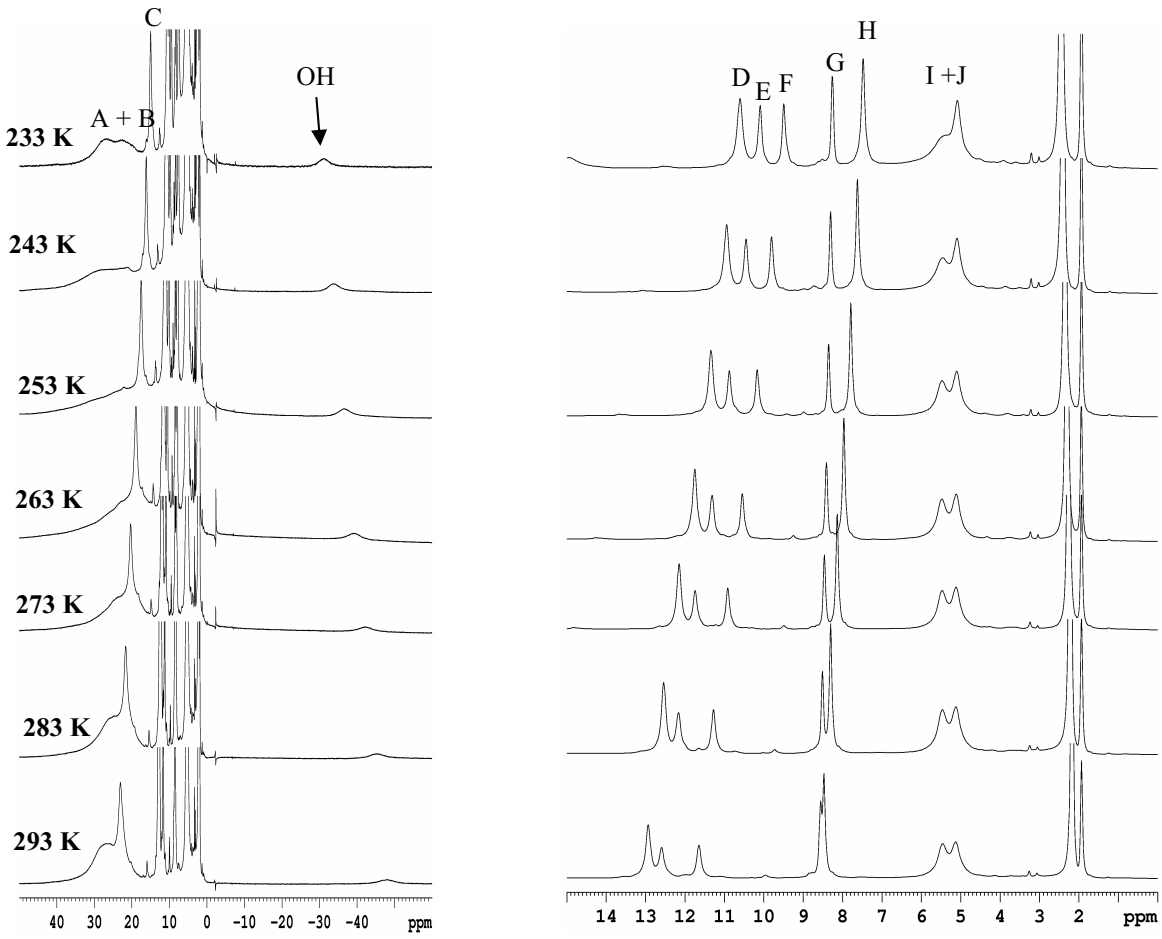

Figure 6.7. The changes in the ^{1}H NMR spectrum (300 MHz, CD_3CN) of **1** in the range 233-293 K. Left: the whole spectrum range (+50 to -60 ppm), enlarged; right: +15 to 0 ppm range.

Careful comparison of the Cu…H contact distances in the crystal structure indicates that the protons H1b and H8b are located significantly closer to Cu^{II} ions than their neighbors H1a and H8a. However, the corresponding resonances I and J are observed very close in the spectrum, which is perhaps caused by a rotational movement of the flexible ethylene groups of the complex cation in solution. The broad resonance A and B with an approximate integral intensity 4 can thus be assigned to the diastereotopic protons of the pyrazolylmethylene moieties, with axial protons experiencing larger hyperfine shifts than equatorial protons.[29] It is believed that the resonance originating from the pyridylmethylene protons, which are closest to copper, is broadened beyond recognition; however, it should emphasized that a possibility of it being hidden under the resonances A and B cannot be ruled out, since the line broadness of the latter resonances makes their integration rather uncertain.

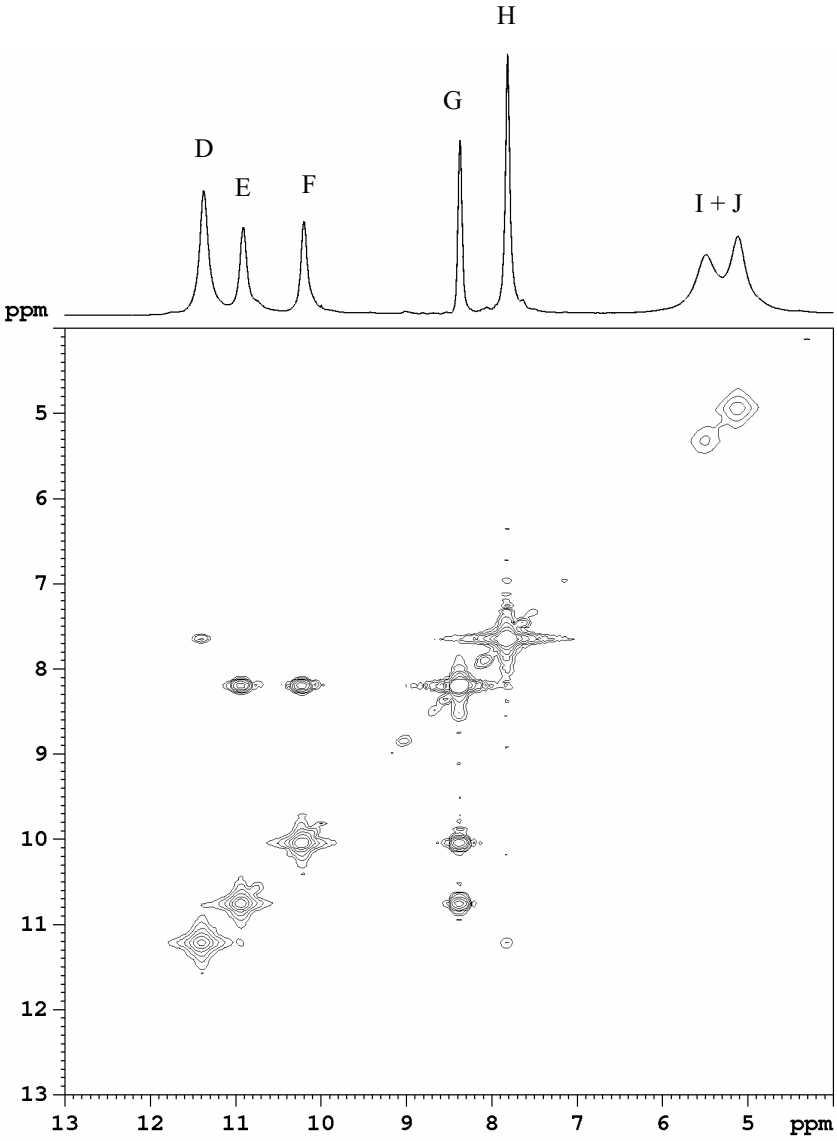

Figure 6.8. 2D COSY spectrum of **1** recorded at 263 K (CD_3CN, 300 MHz), displaying spin-spin connectivities between the resonances D and H, and the resonances E and F and the resonance G.

Further useful information can be obtained from the analysis of the longitudinal relaxation times (T_1). Assuming a predominant dipolar relaxation mechanism as reported by Holz and co-workers[23,25] in spin-coupled dicopper(II) complexes, the Cu…H contact distance *r* should be proportional to $T_1^{1/6}$. Using the equation $r_i = r_{ref}(T_{1i}/T_{1ref})^{1/6}$, in which r_i and T_{1i} are the Cu…H contact distance and the relaxation time of proton *i* and r_{ref} and T_{1ref} are the Cu…H contact distance and the relaxation time of the reference proton, the distances of each proton to the closest Cu^{II} center can be calculated. As a reference proton the γ-proton of the pyridine ring was used, and r_{ref} was taken as an arithmetic average of the Cu…H contact distances of two equivalent γ-protons in the crystal structure. The results are listed in Table 6.3. As can be seen, in general a rather good correlation is observed between the solution-determined Cu…H contact distances and the crystallographic ones, as the discrepancies between the calculated and the observed Cu…H contact distances do not exceed 20%. The differences noted may

originate from slight discrepancies between the solid-state and solution structures, or from electron spin-delocalization and contact interactions within the aromatic rings. However, unfortunately the results do not allow the differentiation between the protons of the aromatic rings, *e.g.* 4' and 5' protons of the pyrazole rings and 3' and 5' protons of the pyridine rings.

Resonance C, which does not show any cross peaks in the 2D COSY spectrum, probably due to its large line width, has been assigned to the 6' pyridine protons by default. The lack of a cross-peak in 2D COSY NMR is not uncommon for α-pyridine protons of paramagnetic Cu^{II} complexes.[23,25,30] The assignment is consistent with its T_1 and T_2 values (T_1 = 6.7 ms, T_2 = 222 Hz at 233 K), and its relatively large downfield shift in comparison to the other pyridine signals, due to its close proximity to the copper(II) ions.

Table 6.3. Longitudinal (T_1) relaxation times and line widths[a] measured at 233 K, and Cu-H distances calculated from the NMR data for **1** and determined from the X-ray structure

Resonance	*T_1, ms*	*Line width, Hz*	*r_{Cu-H}, calc., Å*	*r_{Cu-H}, determ., Å*	*Assignment[d]*
A	5.8	*b*	3.44	3.76	pz–C$\underline{H}_{2(eq)}$-N
B	4.9	*b*	3.34	3.30	pz-C$\underline{H}_{2(ax)}$-N
C	6.7	222	3.52	3.20	6'H-py
D	68.0	46	5.18	4.96	4'H-pz
E	58.8	27	5.06	4.90	3'H-py
F	58.8	23	5.06	5.13	5'H-py
G	132.6	13	5.79	5.79	4'H-py
H	67.3	25	5.17	5.17	5'H-pz
I	8.8	~118[c]	3.69	3.36	Pz-$(CH_2)_2$-pz (H1b +H8b)
J	8.8	~77[c]	3.69	4.61	Pz-$(CH_2)_2$-pz (H1a +H8a)

[a] The line widths are full width at half maximum. [b] Not measured because of broadness. [c] Measured at 253 K due to the signals overlapping at 233 K. [d] See also Figure 6.12.

6.2.4.2 1D NOE difference measurements

In the case of paramagnetic metal complexes, the fast nuclear relaxation rates and the relatively small size of the molecules usually prevent the use of NOE techniques. This is caused by the fact that the NOE intensity in paramagnetic molecules is proportional to the rotational correlation time and inversely proportional to the nuclear relaxation rates.[31] Although 1D NMR techniques, like NOE difference spectroscopy were previously successfully applied for the studies of biological proteins, they are scarcely used for the studies of coordination compounds.[32-36] In the present case, the first example of NOE difference experiments being successfully applied on a

paramagnetic Cu^{II} complex, in attempt to achieve a complete assignment of the resonances corresponding to the protons of the aromatic rings is reported.

Irradiation of the resonances I and J at 263 K, corresponding to the protons of the ethylene moieties of the macrocyclic ring, yields in both cases positive NOE's for both resonances D and H (Figure 6.9). The NOE signal of the latter resonances appears to be of higher intensity; therefore it was tentatively assigned it to the 5' protons of the pyrazole rings, which are located closer in space to the protons of the ethylene moieties. The very weak NOE signal of the resonance D is likely to be caused by spin diffusion. However, an absolute discrimination between these two resonances is unfortunately not possible, as the lower intensity of the NOE signal of the resonance D may also be inherent to its large line width.

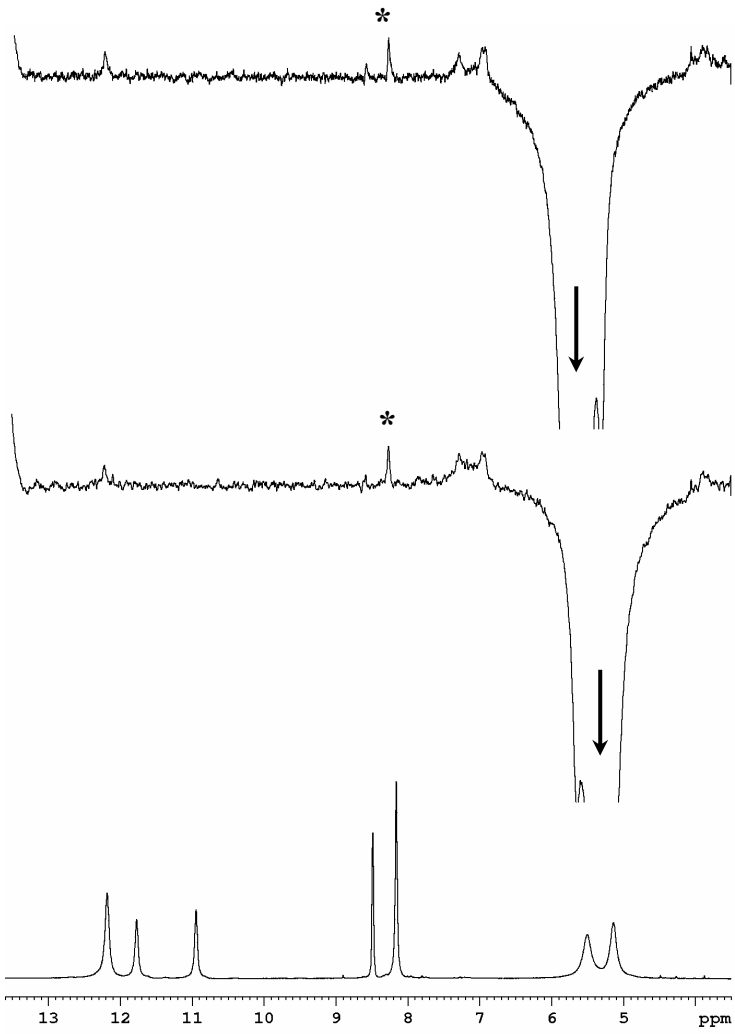

Figure 6.9. NOE difference spectra (CD_3CN, 600 MHz, 263 K), obtained upon irradiation of the resonances I (top) and J (middle). The peak H, which gives a more intense NOE signal, is marked with an asterisk.

It should be mentioned that the NOE connectivities between the pyrazole and ethylene protons are observed only upon irradiation of faster relaxing protons of the ethylene moieties (resonances I and J), but not upon irradiation of slower relaxing

protons of the pyrazole rings (resonances D and H). In the case of the latter protons irradiation, only a positive NOE signal from the neighbor pyrazole proton is observed (Figure 6.10). A similar behavior has been previously reported by Bubacco and co-workers for the Cu^{II} active site of tyrosinase.[37]

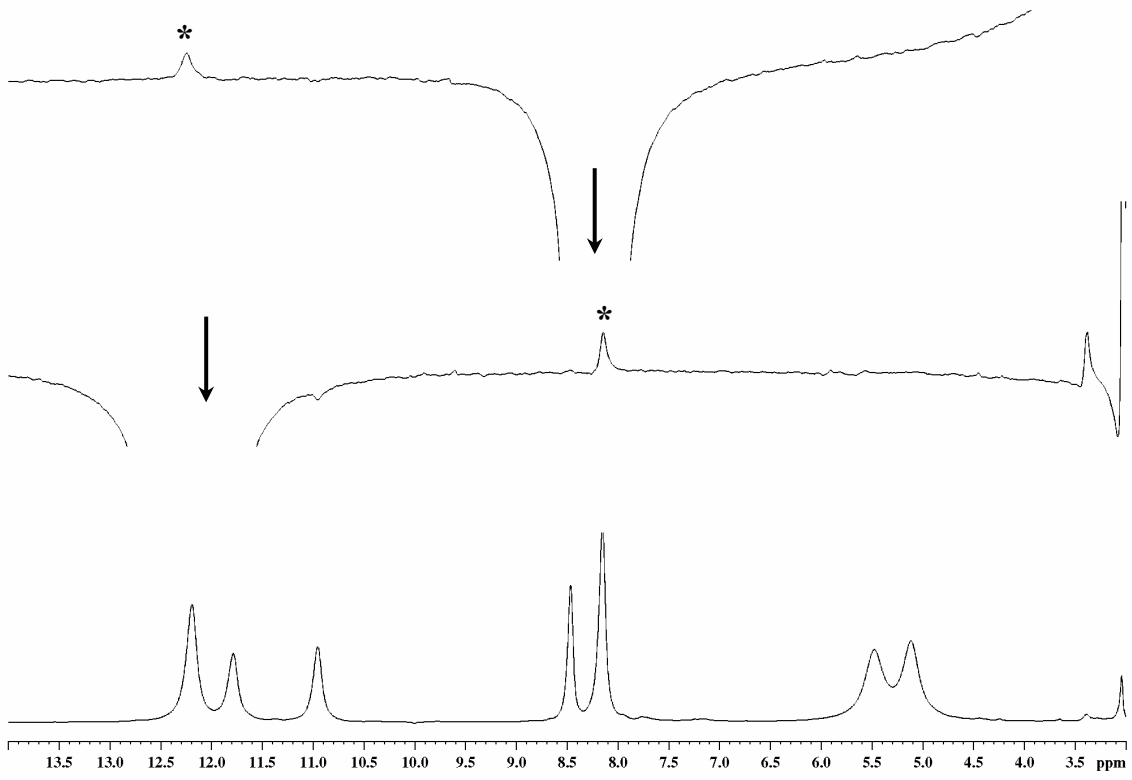

Figure 6.10. NOE difference spectra obtained upon irradiation of the resonances H (top) and D (bottom), corresponding to the pyrazole protons. The neighbor proton of the aromatic ring displays a NOE connectivity to the irradiated signal.

6.2.4.3 Distinguishing between the 3' and 5' protons of the pyridine rings

In the case of the 3' and 5' protons of the pyridine rings, the NOE spectroscopic technique could not be applied, as the only protons closely located to only one of the two considered protons are the protons of the pyridylmethylene moieties and the 6' protons of the pyridine rings. While the protons of the pyridylmethyl moieties are assumed to broaden beyond recognition, the very short T_1 value of the pyridine 6' protons precluded an observation of appreciable NOE connectivities. Therefore, a derivative ligand in which the two 3' protons of the pyridine rings were substituted by methyl groups was prepared. Regretfully, the very light-green compound obtained upon reaction of this ligand with copper(II) perchlorate in the presence of base in acetonitrile, exhibited very broad and poorly resolved resonances in the NMR spectrum in CD_3CN solution. In the UV-Vis spectrum of this solution, the peak at 350 nm, corresponding to the CT band of the bridging OH^- to Cu^{II} ions is absent, suggesting that the hydroxo-bridged complex with the methyl-substituted ligand does not form in acetonitrile.

Fortunately, in D_2O, a reasonably well-resolved NMR spectrum could be recorded, which is shown in Figure 6.11 (bottom). The *in situ* formation of the hydroxo-bridged complex in D_2O was confirmed by UV-Vis and mass spectroscopy (see Experimental part). For comparison, the spectrum of **1** was recorded in water as well (Figure 6.11, top). Although the quality of both spectra is rather poor, not in the least due to a poor solubility of the compounds, the two spectra are very similar. The absence of resonance E in the spectrum of the methylated complex allows its assignment to the 3' protons of the pyridine rings in **1**. Another clear difference between the two spectra is the resolution of the resonances G and H in the spectrum of the complex with the methylated ligand, in contrast to their degeneracy in the spectrum of **1** at RT (Figure 6.11). A very intensive peak of water traces, always present in D_2O, obscures the resonances I and J. A complete assignment of all resonances in ^{1}H NMR spectrum of **1** is shown in Figure 6.12.

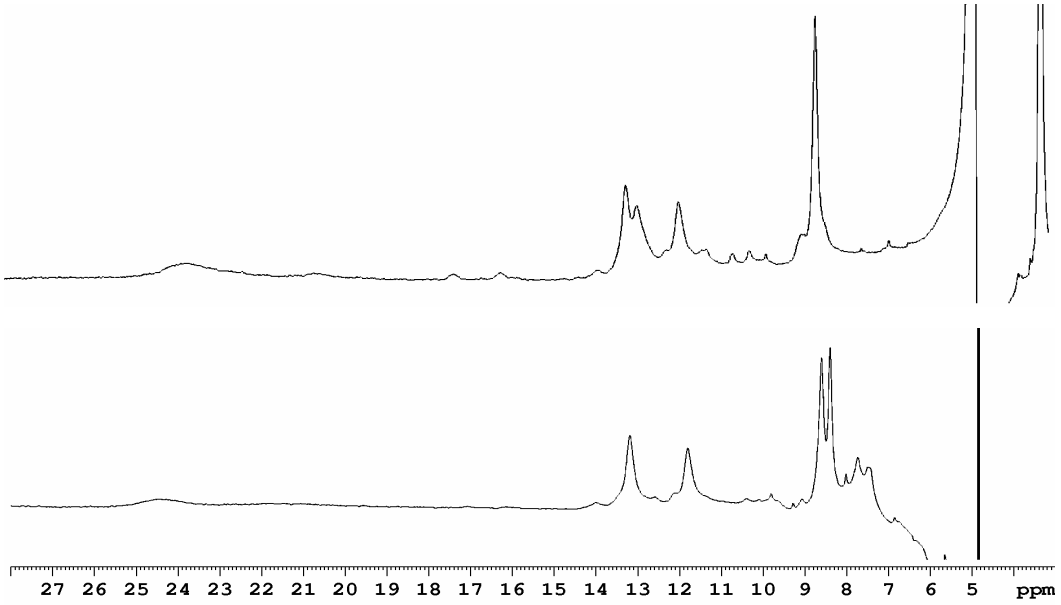

Figure 6.11. The ^{1}H NMR (300 MHz, D_2O) spectra of **1** (top) and **1**-Me_2 (the complex with the macrocyclic ligand containing methyl substituents at the 3' positions of the pyridine rings, *in situ*) (bottom). The measurements were performed with a suppression of H_2O resonance, which causes it being out of phase.

6.2.5 Determination of the antiferromagnetic coupling constant *J* from the temperature-dependent NMR studies on 1

The temperature dependencies of the observed hyperfine-shifted NMR signals of **1** were recorded over the temperature range of 233-353 K. As can be seen from Figure 6.7, the resonances shift downfield with increasing temperature, the complex thus showing an anti-Curie behavior. As shown previously, the type of behavior in the antiferromagnetically coupled Cu^{II} complexes was found to be dependent on the order

of magnitude of the magnetic coupling constant J.[38] The antiferromagnetic coupling creates a dicopper(II) system in which the ground state ($S = 0$) is separated from the first excited ($S = 1$) state by $2J$.[39] A very elegant study reported by Shokhirev and Walker[40] takes into account the temperature-dependent change in the population of the excited state. This approach has been successfully used to evaluate the strength of the spin-coupling interaction for 2Fe-2S clusters and dicopper centers.[41,42] In the present case, the variable temperature data obtained for the hyperfine-shifted signals were simultaneously fitted (Figure 6.13) using the program TDWf, kindly provided by N. Shokirev and A. Walker.[40] The fitting resulted in a $2J$ value of -729(22) cm^{-1}. A relatively large error margin is due to the fitting of a limited temperature range, as dictated by the freezing and boiling temperatures of the solvent. Still, the obtained value is in perfect agreement with the exchange constant obtained from the magnetic susceptibility studies ($2J$ = -691(35) cm^{-1}). This result clearly demonstrates the possibility and power to use NMR spectroscopy to probe the magnetic properties of coordination compounds with unpaired electrons in solution.

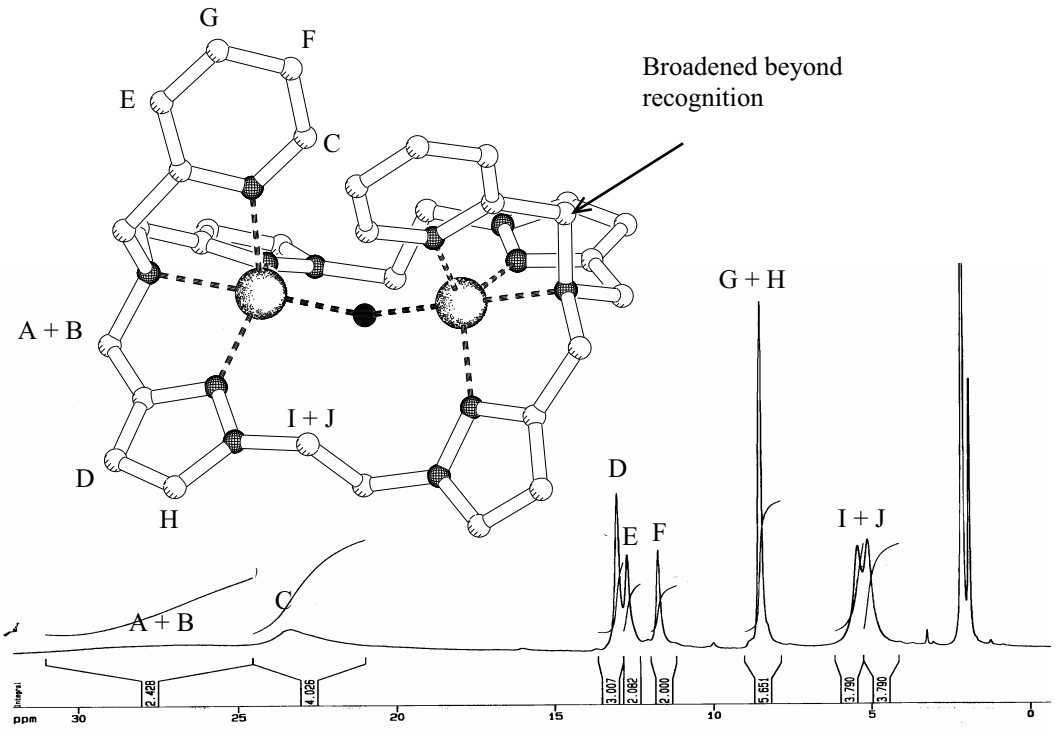

Figure 6.12. An assignment of the resonances in ^{1}H NMR spectrum of **1** (see also Table 6.3).

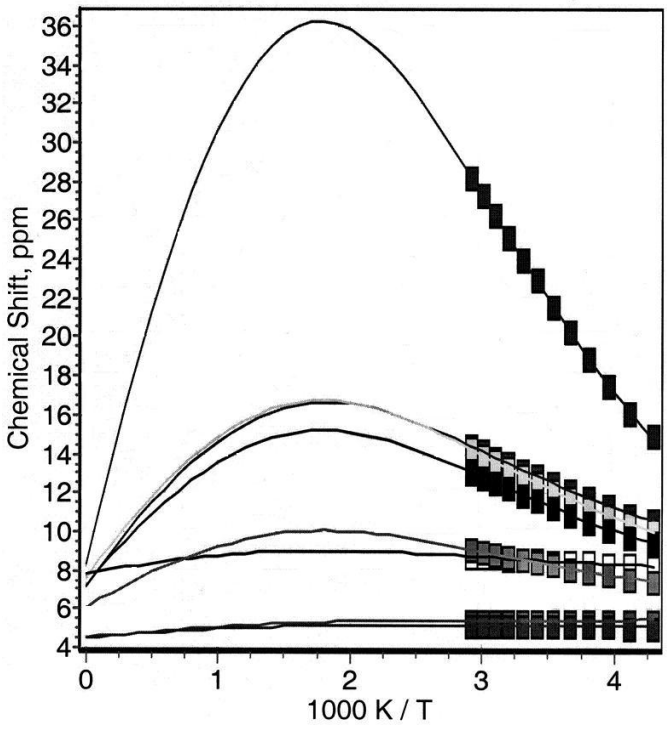

Figure 6.13. Plot of the chemical shifts of **1** in the temperature range of 233-353 K *vs.* the reciprocal temperature (1000 K/T). The simultaneous fitting for eight resonances by the program TDWf[40] results in $2J = -729(22)$ cm^{-1}.

6.3 Concluding remarks

In conclusion, a mono-hydroxo bridge mediates an antiferromagnetic coupling between the metal centers in dinuclear Cu^{II} complexes. The analysis of magneto-structural data for Cu^{II} complexes with a single hydroxo bridge and different coordination geometries around Cu^{II} ions (square-planar, square-pyramidal and trigonal bipyramidal) indicate that in all three cases, a common general trend is present with the strength of antiferromagnetic interaction increasing with longer Cu…Cu separations, wider Cu–O–Cu angles and higher Cu–O–Cu / Cu…Cu ratios.

It can also be concluded that proton NMR spectroscopy is a valuable technique which can be successfully applied on paramagnetic Cu^{II} complexes, provided that a significant antiferromagnetic coupling is present between the metal ions. The presence of strong antiferromagnetic interactions in a molecule overcomes the problem of long electron relaxation of the Cu^{II} ions, leading to shorter longitudinal (T_1) and transversal (T_2) nuclear relaxation times. As a result, commonly used NMR techniques for diamagnetic molecules, like 2D COSY and 1D NOE difference measurements, can also be successfully applied on Cu^{II} complexes. In particular, the latter spectroscopic technique can potentially be a rich source of structural information in solution. Finally, the strength of the magnetic coupling between the metal ions can be determined rather precisely from solution NMR studies. There is little doubt that NMR spectroscopy will

further develop as one of the most successive tools to study the structural and magnetic properties of paramagnetic molecules in solution.

6.4 Experimental Section

6.4.1 Materials and Methods

All starting materials were commercially available and used as purchased, unless stated otherwise. THF and methanol were dried over Na and distilled under Ar prior to use. The macrocyclic ligand [22]py4pz was synthesized by the previously described procedure,[6] according to the reaction scheme shown in Figure 6.1. The deuterated ligand [22]py4pz-d_8 was synthesized following a similar experimental procedure, starting from the commercially available ethylene glycol-d_4 (see below). The infrared spectrum of **1** in the 4000-300 cm^{-1} range was recorded on a Bruker 330V IR spectrophotometer equipped with a Golden Gate Diamond Set. The ligand field spectrum in solution was recorded on a Varian Cary 50 Scan UV-Vis spectrophotometer. Electrospray mass spectra (ESI-MS) in D_2O solutions were recorded on a Thermo Finnigan AQA apparatus. X-band electron paramagnetic resonance (EPR) measurements were performed at 77 K in the solid state on a Jeol RE2x electron spin resonance spectrometer, using DPPH ($g = 2.0036$) as a standard. Bulk magnetization measurements were performed on polycrystalline sample of **1** in the temperature range 5-400 K with a Quantum Design MPMS-5S SQUID magnetometer, in a 0.1 Tesla applied field. The data were corrected for the experimentally determined contribution of the sample holder. Corrections for the diamagnetic response of the complex, as estimated from Pascal's constants, were applied.[43]

6.4.2 ^{1}H NMR spectroscopic studies

The ^{1}H 1D and 2D COSY NMR spectra were recorded on a DPX300 Bruker spectrometer. All chemical shifts were reported with respect to the residual solvent peak. The longitudinal relaxation times (T_1) were determined by standard inversion-recovery experiments, with 2 s relaxation delay and the spectral width of 99.7582 ppm. The COSY spectrum was obtained at 263 K by collecting 1024 F_2×1024 F_1 data points, with a relaxation delay of 0.02 s and the spectral width of 34.0678 ppm. 384 scans were collected. The NOE difference spectra were recorded on a DMX600 Bruker spectrometer. 1D NOE difference experiments were performed by a literature procedure,[44,45] using a frequency list to define irradiation frequencies, alternating on and off resonance every other scan. A WEFT pulse sequence was not applied. The irradiation time was 500 ms. The number of scans during the experiments was 4 k.

6.4.3 Ligand synthesis

1,2-bis-tosylate-ethane-d_4: The compound was synthesized in the same way as its non-deuterated analogue, starting from commercially available ethylene glycol-d_4.[6] Yield: 82.8%. ^{1}H NMR (300 MHz, DMSO, ppm): δ = 7.71 (d, 4H, Ar-(*o*)-H); 7.45 (d, 4H, Ar-(*m*)-H); 2.44 (s, 6H, Ar-CH_3).

1,2-di(3-formyl-1-pyrazolyl)ethane-d_4: The compound was synthesized as a white solid by the same method as its non-deuterated analogue.[6] Yield: 58%. ^{1}H NMR (300 MHz, $CDCl_3$, ppm): δ = 9.97 (s, 2H, C(O)H); 7.08 (d, 2H, 4'pz-H); 6.69 (d, 2H, 5'pz-H).

1,2-di(3-hydroxymethyl-1-pyrazolyl)ethane-d_4: The compound was synthesized by the same method as its non-deuterated analogue and used without purification from borate salts.[6] Yield: not determined (above 100% due to the presence of borate salts). ^{1}H NMR (300 MHz, $CDCl_3$, ppm): δ = 7.13 (d, 2H, 4'pz-H); 6.16 (d, 2H, 5'pz-H); 4.54 (s, 4H, pz-CH_2-OH).

1,2-di(3-chloromethyl-1-pyrazolyl)ethane-d_4: The compound was synthesized according to a slight modification of the procedure reported by Schuitema *et al.*[6] The white solid obtained in the synthesis of 1,2-di(3-hydroxymethyl-1-pyrazolyl)ethane-d_4 was dissolved in 100 ml of thionyl chloride and heated at 50 °C upon stirring for 24 hours. Afterwards, $SOCl_2$ was evaporated under reduced pressure, and the residue was neutralized with saturated aqueous solution of Na_2CO_3. The product was extracted with dichloromethane. The organic phase was dried upon Na_2SO_4, and evaporated under reduced pressure. The product was recrystallized from methanol. Yield: 45% (relative to 1,2-di(3-formyl-1-pyrazolyl)ethane-d_4). ^{1}H NMR (300 MHz, $CDCl_3$, ppm): δ = 6.90 (d, 2H, 4'pz-H); 6.16 (d, 2H, 5'pz-H); 4.59 (s, 4H, pz-CH_2-Cl).

1,2-di-(3'-(2-pyridylmethylamino)-1'-pyrazolyl)ethane-d_4 (py2pz-d_4): The compound was synthesized according to the procedure used for its non-deuterated analogue.[6] Yield: 64%. ^{1}H NMR (300 MHz, $CDCl_3$, ppm): δ = 8.53 (d, 2H, 6'H-py), 7.63 (td, 2H, 4'H-py); 7.34 (d, 2H, 3'H-py); 7.13 (td, 2H, 5'H-py), 6.90 (d, 2H, 5'H-pz); 6.08 (d, 2H, 4'H-pz); 3.95(s, 4H, py-CH_2-N); 3.85 (s, 2H, pz-CH_2-N).

9,22-bis(2-pyridylmethyl)-1,4,9,14,17,22,27,28,29,30-decaazapentacycle [22.2.1.14,7.111,14.117,20]triacontane-5,7(28),11(29),12,18,20(30),24(27),25-octaene ([22]py4pz-d_8): The compound was synthesized according to a slight modification of the procedure earlier reported by Schuitema *et al.*[6] 0.301 g (2.84 mmol) of sodium carbonate and 0.577 g (1.42 mmol) of py2pz-d_4 were suspended in 3000 ml of dry THF. The reaction mixture was cooled to -40 °C, and a solution of 0.374 g (1.42 mmol) of 1,2-di(3'-chloromethylpyrazol-1'-yl)ethane-d_4 in *ca.* 200 ml of THF was added. The reaction mixture was allowed to warm slowly to RT and was then refluxed for 14 days under Ar. After two weeks, the solvent was evaporated, and the residue was redissolved in *ca.* 500 ml of a CH_2Cl_2-water mixture (1:1 v:v). The aqueous phase was acidified

with 35% HCl (till pH = 1) and washed a few times with dichloromethane. Afterwards, the aqueous layer was basified with NH_4OH (pH = 9), and the product was extracted a few times with dichloromethane. The combined organic layers were dried over Na_2SO_4, and the solvent was evaporated. The obtained yellow oil was redissolved in methanol, and the product was precipitated with diethyl ether. Yield: 27%. ^{1}H NMR (300 MHz, $CDCl_3$, ppm): δ = 8.40 (d, 2H, 6'H-py), 7.81 (td, 2H, 4'H-py); 7.64 (d, 2H, 3'H-py); 7.41 (d, 2H, 5'H-pz); 7.25 (td, 2H, 5'H-py); 6.11 (d, 2H, 4'H-pz); 3.56 (s, 4H, py-CH_2-N); 3.36 (s, 2H, pz-CH_2-N).

3-methyl-2-pyridylmethylamine: The compound was synthesized according to a slight modification of the procedure reported earlier by Fos *et al.*[46] 1 g (8.5 mmol) of 2-cyano-3-methylpyridine was dissolved in 200 ml of dry MeOH and hydrogenated with molecular hydrogen in the presence of 1.5 g of 10% Pd on a charcoal. After 6 hours, the charcoal was filtered off, and 4 ml of concentrated HCl was added to the resulting solution. After evaporation, a mixture of white crystals of product and some amount of light yellow oil was obtained. The product was recrystallized from a MeOH-diethyl ether mixture. Yield: 0.70 g (42 %). ^{1}H NMR (MeOD, 300 MHz, ppm): δ = 8.64 (d, 1H, 2'H-py); 8.14 (d, 1H, 4'H-py), 7.69 (dd, 1H, 3'H-py), 4.45 (s, 2H, CH_2py), 2.52 (s, 3H, CH_3).

1,2-di-(3'-(3-methyl-2-pyridylmethylamino)-1'-pyrazolyl)ethane (py2Me$_2$pz): Under an argon atmosphere, 0.38 g (1.78 mmol) of 1,2-di(3-formyl-1-pyrazolyl)ethane and 1.2 ml (4 equivalents) of diisopropylethylamine (DIPEA) were dissolved in 400 ml of dry methanol. A solution of 0.68 g (3.46 mmol) of 3-methylpyridin-2-ylmethylamine in 50 ml of dry MeOH was added dropwise to the reaction mixture. The purity of the imine, which immediately forms *in situ*, was checked by NMR spectroscopy, and its reduction was carried out without isolating the compound. $NaBH_4$ (3 eq/CH=N bond) was added to the solution. After the evolution of gas stopped, the resulting mixture was refluxed for two hours and the solvent was evaporated under reduced pressure. The residue was dissolved in *ca.* 250 ml of a biphasic H_2O-dichloromethane mixture, and the organic layer was separated. After washing the aqueous layer a few more times with dichloromethane, the organic layers were combined, dried over Na_2SO_4 and evaporated. This work-up resulted in the pure product as a light yellow oil. Yield: 0.47 g (61 %). ^{1}H NMR ($CDCl_3$, 300 MHz), ppm: δ = 8.39 (d, 2H, 6'H-py), 7.41 (d, 2H, 4'H-py), 7.06 (dd, 2H, 5'H-py), 6.90 (d, 2H, 3'H-pz), 6.08 (d, 2H, 4'H-pz), 4.47 (s, 4H, pz-(CH_2)$_2$-pz), 3.90 (s, 8H, NH-CH_2-py + NH-CH_2-pz), 2.32 (s, 6H, CH_3-py).

9,22-bis(3-methyl-2-pyridylmethyl)-1,4,9,14,17,22,27,28,29,30-decaazapentacycle[22.2.1.14,7.111,14.117,20]triacontane-5,7(28),11(29),12,18,20(30),24(27),25-octaene ([22]pyMe$_2$4pz): Under an argon atmosphere, 0.343 g (3.24 mmol) of Na_2CO_3 and 0.696 g (1.62 mmol) of py2Me$_2$pz were suspended in 3500 ml of dry THF. *Ca.* 200 ml of CH_3CN was added to ensure the

dissolution of the organic compound. The suspension was cooled down to -20 °C, and a solution of 0.419 g (1.62 mmol) of 1,2-di(3'-chloromethyl-1'-pyrazolyl)ethane in 100 ml of dry THF was added to the reaction mixture. The resulting suspension was allowed to warm slowly to room temperature, and refluxed for two weeks under argon. Afterwards, the solvent was evaporated, and the residue was redissolved in a dichloromethane-water mixture. The organic layer was separated, and the aqueous layer was washed three more times with dichloromethane. The product was extracted by a diluted HCl solution, and the resulting aqueous solution was washed a few more times with dichloromethane. Addition of an ammonium hydroxide solution till pH = 11 resulted in the formation of a white suspension, which was extracted four times with dichloromethane. The resulting organic solution was dried over Na_2SO_4 and evaporated under reduced pressure. The resulting crude product, obtained as a dark-brown oil, was purified by column chromatography on silica, using CH_2Cl_2:MeOH mixture (85:15, v:v) as an eluent. The pure ligand was crystallized from a MeOH/diethyl ether solution and isolated as a white powder. Yield: < 10%. ^{1}H NMR (300 MHz, MeOD, ppm): δ = 8.35 (d, 2H, 6'H-py); 7.68 (d, 2H, 4'H-py); 7.49 (d, 2H, 5'H-pz); 7.29 (d, 2H, 5'H-py); 6.19 (d, 4H, 4'H-pz); 4.57 (s, 16H, pz-(CH_2)$_2$-pz + pz-(CH_2)-N); 3.69 (s, 4H, py-CH_2-N); 2.28 (s, 6H, CH_3-pz)

6.4.4 Syntheses of the coordination compounds

[Cu_2([22]py4pz)(μ-OH)](ClO_4)$_3$·H_2O (1): A solution of $Cu(ClO_4)_2·6H_2O$ (74 mg, 0.20 mmol) in *ca.* 2 ml acetonitrile was added to a suspension of [22]py4pz (58 mg, 0.10 mmol) in the same solvent (the free ligand does not dissolve, unless coordinated to the metal ions). To the resulting greenish-blue solution one equivalent of NMe_4OH (20% solution in methanol) was added, which resulted in an immediate color change to clear green. Small amounts of copper hydroxide that may precipitate occasionally were removed by filtration. The resulting clear solution was concentrated to the half of its initial volume. Diethyl ether diffusion led to small green crystals, which were isolated and recrystallized from an acetonitrile/diethyl ether mixture. Single crystals were obtained by slow diffusion of diethyl ether into a diluted acetonitrile solution of **1**. Elemental analysis, % found (calc.) for [Cu_2([22]py4pz)(μ-OH)](ClO_4)$_3$·H_2O (=$C_{32}H_{39}Cl_3Cu_2N_{12}O_{14}$): C, 36.6 (36.6), H, 3.7 (3.3), N, 16.0 (15.6). IR (4000-300 cm^{-1}), ν: 3514 (O-H stretching), 3126 (C-H arom. stretching), 1610 (C=N arom. pyridine), 1515 (C=N arom. pyrazole), 1076 (ClO_4^-)

[Cu_2([22]py$Me_2$4pz)(μ-OH)](ClO_4)$_3$·H_2O (1-Me_2) (*in situ*): A solution of $Cu(ClO_4)_2·6H_2O$ (7.2 mg, 0.019 mmol) in *ca.* 1 ml acetonitrile was added to a suspension of [22]py$Me_2$4pz (6.0 mg, 0.010 mmol) in the same solvent (the ligand does not dissolve without coordination to metal ions). To the resulting green solution one equivalent of NMe_4OH (20% solution in methanol) was added, which resulted in an immediate color change to greenish-yellow. The resulting solution was concentrated till

the half of its initial volume. Diethyl ether diffusion led to the formation of a very light-green amorphous powder, which was redissolved in D_2O and used for the NMR spectroscopic studies. The *in situ* formation of the hydroxo-bridged complex was confirmed by ESI-MS measurements (D_2O, m/z 529 (1 [22]py$Me_2$4pz + 2 Cu + 1 OH + 3 ClO_4, z = 2; 1078 (1 [22]py$Me_2$4pz + 2Cu + 1 OH + 3 ClO_4 + D_2O, z = 1) and UV-Vis spectroscopy (in D_2O, λ = 350 nm (CT $Cu^{II} \leftarrow$ OH).

Safety Note: Although no problems were encountered during the preparation of perchlorate salts, these compounds are potentially hazardous and should be treated with care.

6.4.5 X-ray crystallographic measurements

X-ray diffraction intensities of **1** were measured on a Bruker AXS Apex diffractometer with graphite monochromator. The structure was solved with direct methods (SHELXS97).[47] The structure refinement was done with SHELXL97[48] against F^2 of all reflections. Molecular illustration, checking for higher symmetry and geometry calculations were performed with the PLATON[49] package. $C_{32}H_{39}Cl_3\ Cu_2N_{12}O_{14}$, Fw = 1049.19, green block (0.07×0.05×0.04 mm^3), a = 21.826(4) Å, b = 12.189(2) Å, c = 17.687(4) Å, β = 117.47(3)°, Z = 4, V = 4174.9(18) $Å^3$, $\rho_{calcd.}$ = 1.666 $g \cdot cm^{-3}$, μ = 1.291 mm^{-1}, monoclinic, space group *C2/c* (no. 15), 21343 reflections collected, 5187 independent reflections (R_{int} = 0.0540). The final cycle of full-matrix least-squares refinement, including 289 parameters, converged into R_1 = 0.0512 (R_1 = 0.0923 all data) and wR_2 = 0.1344 (wR_2 = 0.1447 all data) with a maximum (minimum) residual electron density of 0.887 (-0.499) $e \cdot Å^3$.

6.5 References

(1) Torelli, S.; Belle, C.; Gautier-Luneau, I.; Pierre, J. L.; Saint-Aman, E.; Latour, J. M.; Le Pape, L.; Luneau, D. *Inorg. Chem.* **2000**, *39*, 3526-3536.
(2) Torelli, S.; Belle, C.; Hamman, S.; Pierre, J. L.; Saint-Aman, E. *Inorg. Chem.* **2002**, *41*, 3983-3989.
(3) Ackermann, J.; Meyer, F.; Kaifer, E.; Pritzkow, H. *Chem. Eur. J.* **2002**, *8*, 247-258.
(4) Mukherjee, J.; Mukherjee, R. *Inorg. Chim. Acta* **2002**, *337*, 429-438.
(5) Koval, I. A.; Huisman, M.; Stassen, A. F.; Gamez, P.; Roubeau, O.; Belle, C.; Pierre, J. L.; Saint-Aman, E.; Luken, M.; Krebs, B.; Lutz, M.; Spek, A. L.; Reedijk, J. *Eur. J. Inorg. Chem.* **2004**, 4036-4045.
(6) Schuitema, A. M.; Aubel, P. G.; Koval, I. A.; Engelen, M.; Driessen, W. L.; Reedijk, J.; Lutz, M.; Spek, A. L. *Inorg. Chim. Acta* **2003**, *355*, 374-385.
(7) Schuitema, A. M. Ph.D. thesis, Leiden University, 2004.
(8) Klabunde, T.; Eicken, C.; Sacchettini, J. C.; Krebs, B. *Nat. Struct. Biol.* **1998**, *5*, 1084-1090.
(9) Addison, A. W.; Rao, T. N.; Reedijk, J.; van Rijn, J.; Verschoor, G. C. *J. Chem. Soc., Dalton Trans.* **1984**, 1349-1356.
(10) Kahn, O. *Molecular Magnetism*; Wiley-VCH: New York, 1993.
(11) Patra, A. K.; Ray, M.; Mukherjee, R. *Polyhedron* **2000**, *19*, 1423-1428.
(12) Haddad, M. S.; Wilson, S. R.; Hodgson, D. J.; Hendrickson, D. N. *J. Am. Chem. Soc.* **1981**, *103*, 384-391.
(13) Adams, H.; Bailey, N. A.; Collinson, S. R.; Fenton, D. E.; Haring, C. J.; Kitchen, S. J. *Inorg. Chim. Acta* **1996**, *246*, 81-88.
(14) Coughlin, P. K.; Lippard, S. J. *J. Am. Chem. Soc.* **1981**, *103*, 3228-3229.

(15) Lu, Q.; Latour, J.-M.; Harding, C. J.; Martin, N.; Marrs, D. J.; McKee, V.; Nelson, J. *J. Chem . Soc., Dalton Trans.* **1994**, 1471-1478.
(16) Harding, C. J.; McKee, V.; Nelson, J.; Lu, Q. *J. Chem. Soc., Chem. Commun.* **1993**, 1768-1769.
(17) Spodine, E.; Manzur, J.; Garland, M. T.; Kiwi, M.; Peña, O.; Grandjean, D.; Poupet, L. *J. Chem. Soc., Dalton Trans.* **1991**, 365-369.
(18) Drew, M. G. B.; McCann, M.; Martin-Nelson, M. *J. Chem. Soc., Dalton Trans.* **1981**, 1868-1878.
(19) Castro, I.; Faus, J.; Julve, M.; Lloret, F.; Verdaguer, M.; Kahn, O.; Jeannin, S.; Jeannin, Y.; Vaisserman, J. *J. Chem. Soc., Dalton Trans.* **1990**, 2207-2212.
(20) Foldago, J. V.; Coronado, E.; Beltran-Porter, D.; Rojo, T.; Fuertes, J. *J. Chem. Soc., Dalton Trans.* **1989**, 237-241.
(21) Harding, C. J.; Lu, Q.; Malone, J. F.; Marrs, D. J.; Martin, N.; McKee, V.; Nelson, J. *J. Chem. Soc., Dalton Trans.* **1995**, 1739-1747.
(22) Asato, E.; Toftlund, H.; Kida, S.; Mikuriya, M.; Murray, K. S. *Inorg. Chim. Acta* **1989**, *165*, 207-214.
(23) Holz, R. C.; Brink, J. M. *Inorg. Chem.* **1994**, *33*, 4609-4610.
(24) Murthy, N. N.; Karlin, K. D.; Bertini, I.; Luchinat, C. *J. Am. Chem. Soc.* **1997**, *119*, 2156-2162.
(25) Brink, J. M.; Rose, R. A.; Holz, R. C. *Inorg. Chem.* **1996**, *35*, 2878-2885.
(26) Banci, L.; Bertini, I.; Luchinat, C. *Struct. Bonding* **1990**, *72*, 113-135.
(27) Satcher, J. H. J.; Balch, A. L. *Inorg. Chem.* **1995**, *34*, 3371-3373.
(28) Aromi, G.; Gamez, P.; Kooijman, H.; Spek, A. L.; Driessen, W. L.; Reedijk, J. *Eur. J. Inorg. Chem.* **2003**, 1394-1400.
(29) Belle, C.; Bougault, C.; Averbuch, M.-T.; Durif, A.; Pierre, J. L.; Latour, J. M.; Le Pape, L. *J. Am. Chem. Soc.* **2001**, *123*, 8053-8066.
(30) Lubben, M.; Hage, R.; Meetsma, A.; Bijma, K.; Feringa, B. L. *Inorg. Chem.* **1995**, *34*, 2217-2224.
(31) Bertini, I.; Luchinat, C. *NMR of Paramagnetic Molecules in Biological Systems*; Benjamin/Cummings: Menlo Park, CA, 1986.
(32) Epperson, J. D.; Ming, L.-J.; Woosley, B. D.; Baker, G. R.; Newkome, G. R. *Inorg. Chem.* **1999**, *38*, 4498-4502.
(33) Epperson, J. D.; Ming, L.-J.; Baker, G. R.; Newkome, G. R. *J. Am. Chem. Soc.* **2001**, *123*, 8583-8592.
(34) Dolores Santana, M.; Rufete, A.; Sanchez, G.; Garcia, G.; Lopez, G.; Casabo, J.; Molins, E.; Miravitlles, C. *Inorg. Chim. Acta* **1997**, *255*, 21-27.
(35) Momot, K. I.; Walker, F. A. *J. Phys. Chem. A* **1997**, *101*, 9207-9216.
(36) Lisowski, J.; Latos-Grazynski, L.; Szterenberg, L. *Inorg. Chem.* **1992**, *31*, 1933-1940.
(37) Bubacco, L.; Saldago, J.; Tepper, A. W. J. W.; Vijgenboom, E.; Canters, G. W. *FEBS Letters* **1999**, *442*, 215-220.
(38) Holz, R. C.; Brink, J. M.; Rose, R. A. *J. Magn. Res. A* **1996**, *119*, 125-128.
(39) Holz, R. C.; Alvarez, M. L.; Zumft, W. G.; Dooley, D. M. *Biochemistry* **1999**, *38*, 11164-11171.
(40) Shokhirev, N. V.; Walker, F. A. *J. Phys. Chem.* **1995**, *99*, 17795-17804.
(41) Holz, R. C.; Bennett, B.; Chen, G.; Ming, L.-J. *J. Am. Chem. Soc.* **1998**, *120*, 6329-6335.
(42) Holz, R. C.; Small, F. J.; Ensign, S. A. *Biochemistry* **1997**, *36*, 14690-14696.
(43) Kolthoff, I. M.; Elving, P. J. *Treatise on Analytical Chemistry*; Interscience Encyclopedia, Inc.: New York, 1963.
(44) Dugad, L. B.; La Mar, G. N. *Biochemistry* **1990**, *29*, 2263-2271.
(45) Banci, L.; Bertini, I.; Luchinat, C.; Piccioli, M.; Scozzafava, A.; Turano, P. *Inorg. Chem.* **1989**, *28*, 4650-4656.
(46) Fos, E.; Bosca, F.; Mauleon, D.; Carganico, G. *J. Heterocyclic Chem.* **1993**, *30*, 473-476.
(47) Sheldrick, G. M.; *SHELXS-97, Program for crystal structure solution*. University of Göttingen, Germany, 1997
(48) Sheldrick, G. M.; *SHELXL-97, Program for the refinement of crystal structures*. University of Göttingen, Germany, 1997
(49) Spek, A. L. *J. Appl. Cryst.* **2003**, *36*, 7-13.